SUPPORTING INFORMATION FOR

Design, synthesis and *in vivo* evaluation of 3-arylcoumarin derivatives of rhenium(I) tricarbonyl complexes as potent antibacterial agents against methicillin-resistant *Staphylococcus aureus* (MRSA)

Sara Nasiri Sovari [1], Sandra Vojnovic [2], Sanja Skaro Bogojevic [2], Aurelien Crochet [1], Aleksandar Pavic [2*], Jasmina Nikodinovic-Runic [2*] and Fabio Zobi [1*]

[1] Department of Chemistry, University of Fribourg, Chemin du Musée 10, 1700 Fribourg, Switzerland.

[2] Institute of Molecular Genetics and Genetic Engineering, University of Belgrade, Vojvode Stepe 444a, 11000 Belgrade, Republic of Serbia.

*To whom all the correspondence should be addressed.

Phone (+41) 26 300 87 85, Fax (+41) 26 300 97 37, E-mail : fabio.zobi@unifr.ch

E-mail : sasapavic@imgge.bg.ac.rs

Table of contents

NMR spectra

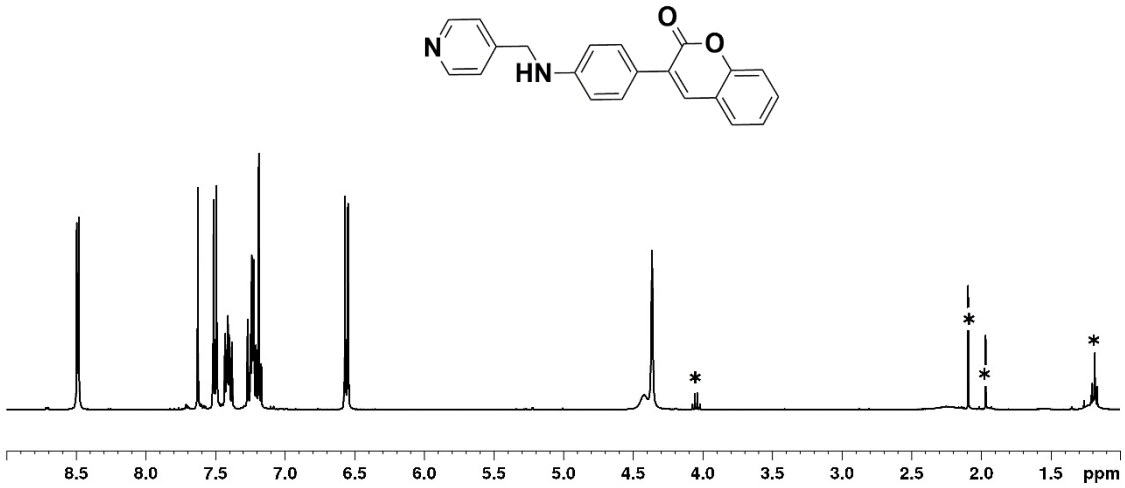

Figure S1. 400 MHz ^{1}H-NMR of L1 (in $CDCl_3$, ✻= solvent residual peak)

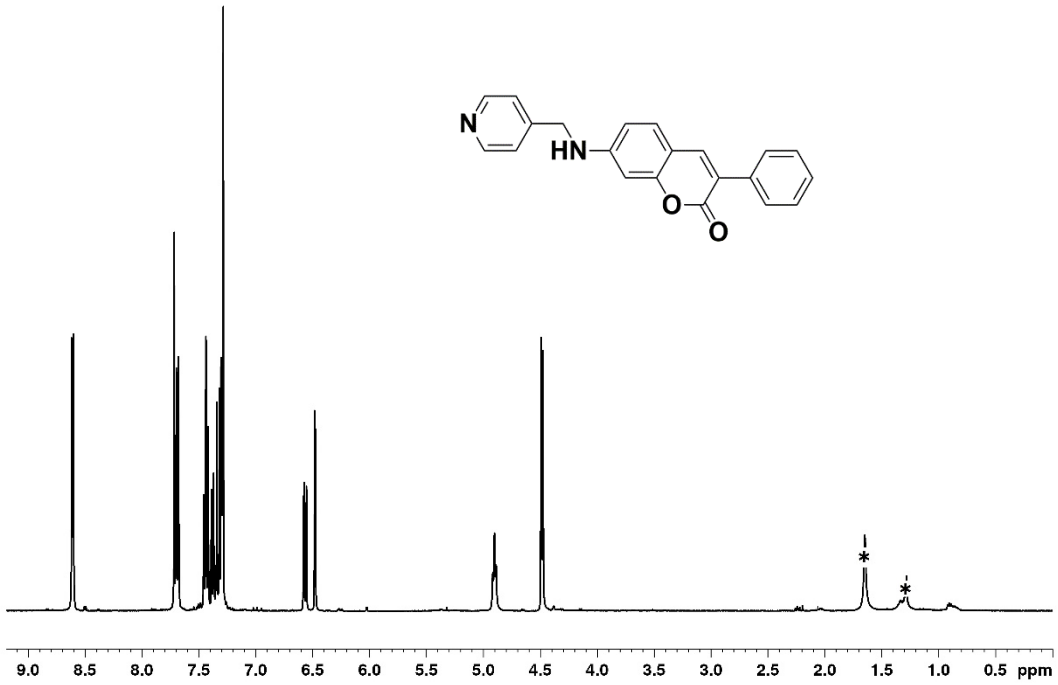

Figure S2. 400 MHz ^{1}H-NMR of **L_2** (in $CDCL_3$, ✱= solvent residual peak)

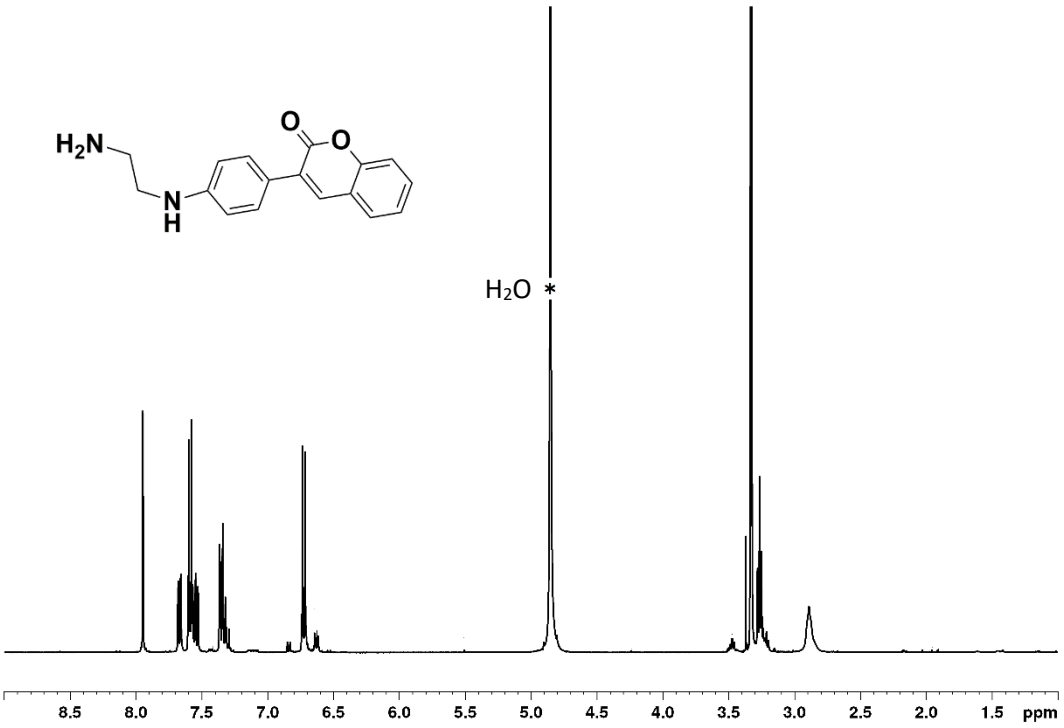

Figure S3. 400 MHz ^{1}H-NMR of **L$_3$** (in MeOH, ✱ = solvent residual peak)

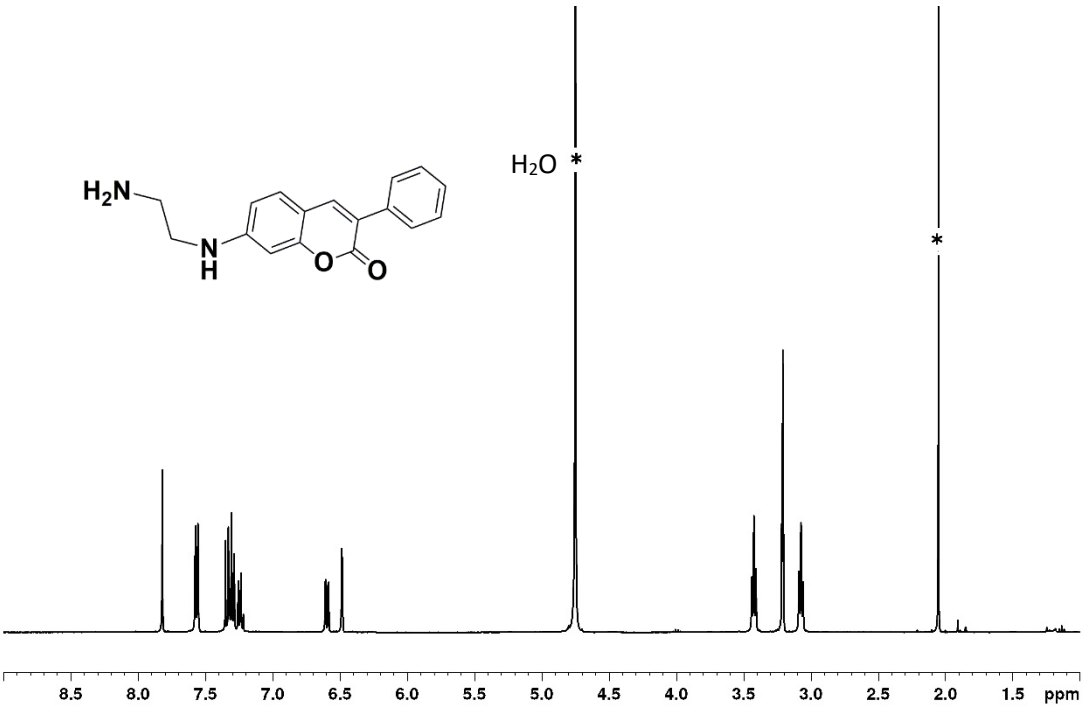

Figure S4. 400 MHz ^{1}H-NMR of **L$_4$** (in MeOH, ✱ = solvent residual peak)

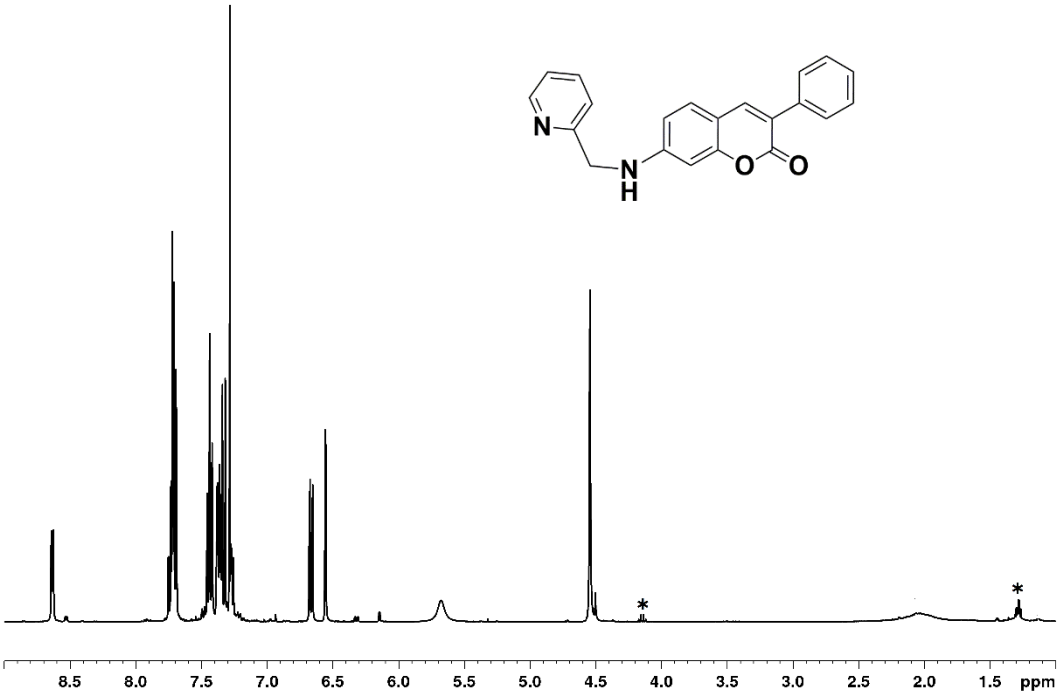

Figure S5. 400 MHz ^{1}H-NMR of **L$_5$** (in $CDCL_3$, ✱ = solvent residual peak)

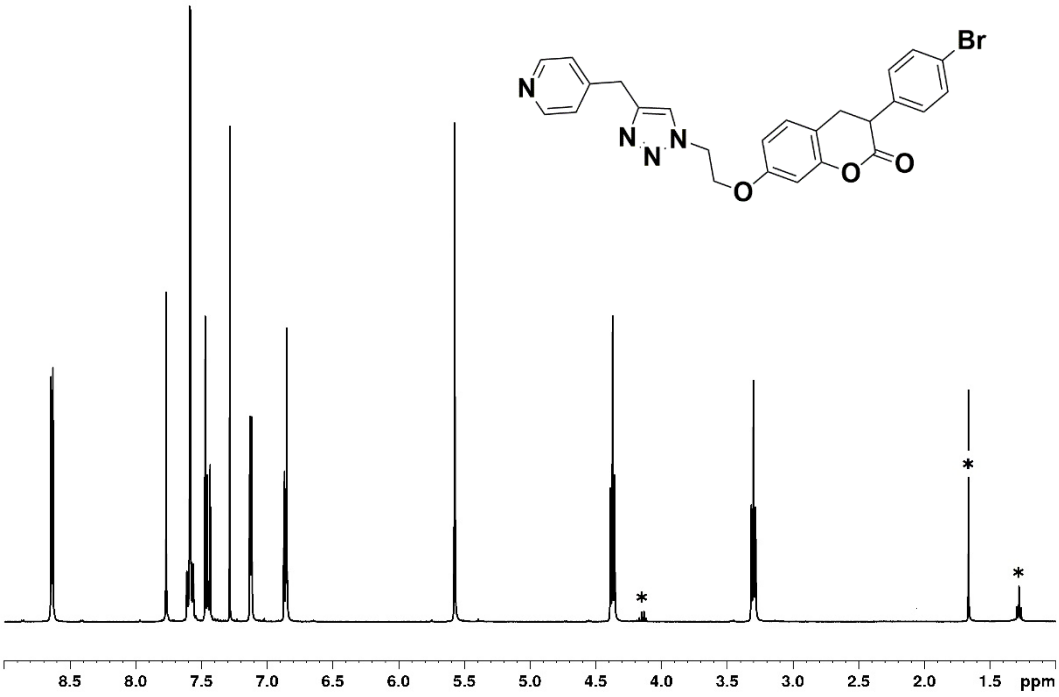

Figure S6. 400 MHz ^{1}H-NMR of **L$_6$** (in $CDCL_3$, ✱ = solvent residual peak)

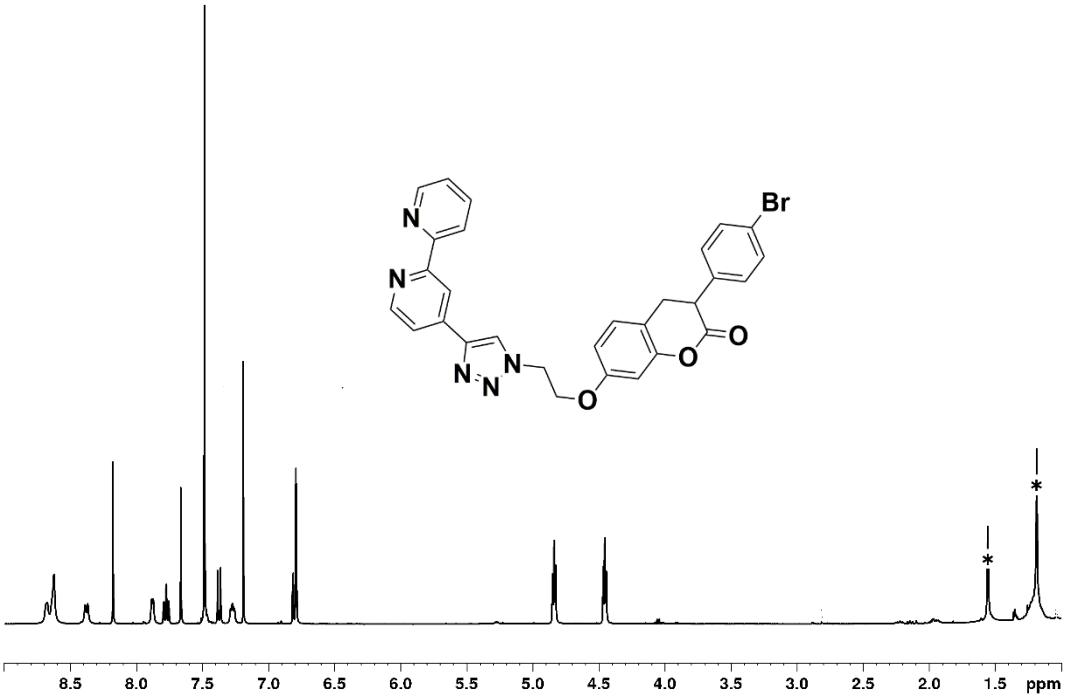

Figure S7. 400 MHz ^{1}H-NMR of **L$_7$** (in $CDCL_3$, ✱ = solvent residual peak)

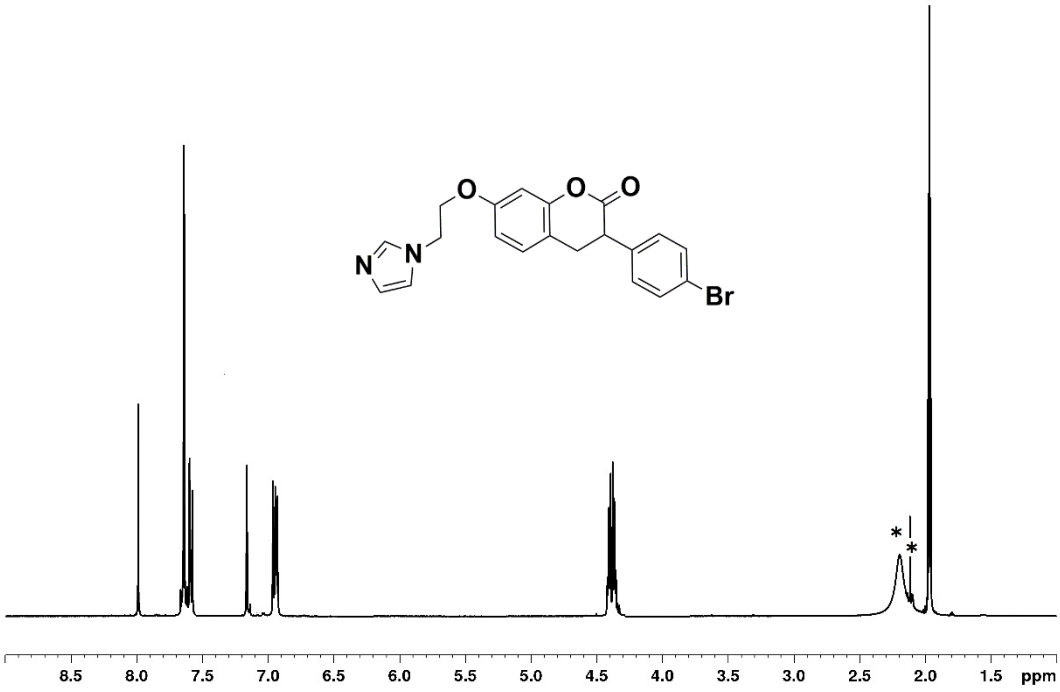

Figure S8. 400 MHz ^{1}H-NMR of **L$_8$** (in CD_3CN, ✱ = solvent residual peak)

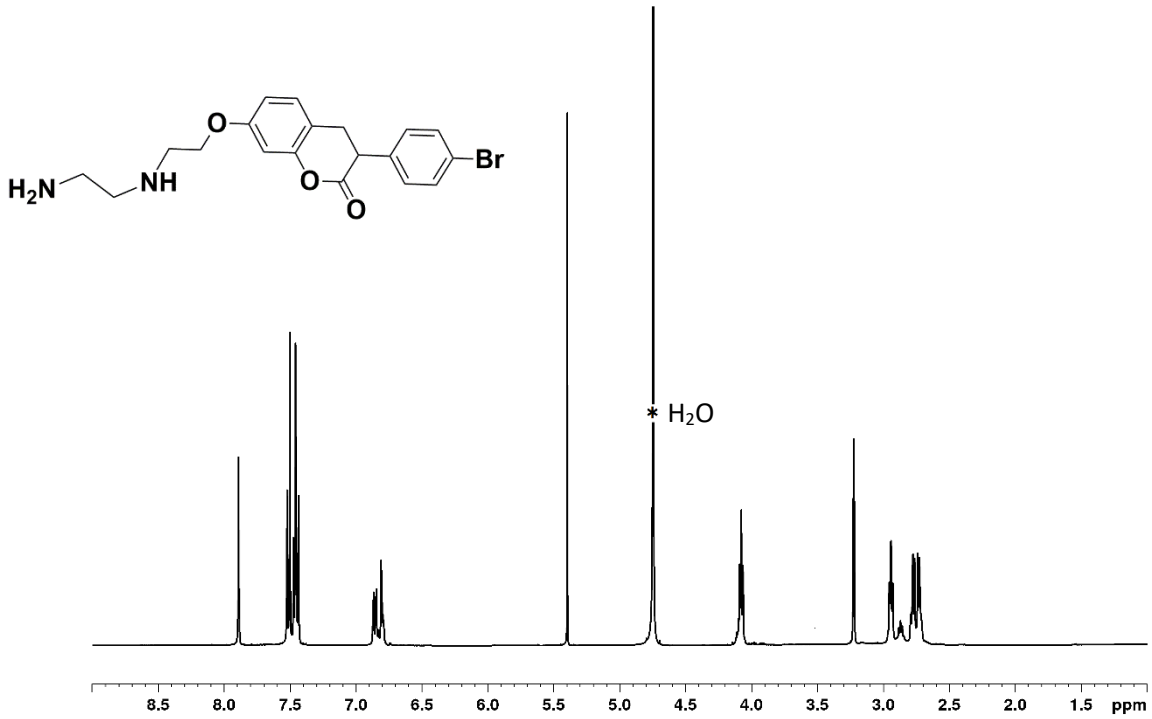

Figure S9. 400 MHz ^{1}H-NMR of **L$_9$** (in MeOH, ✱ = solvent residual peak)

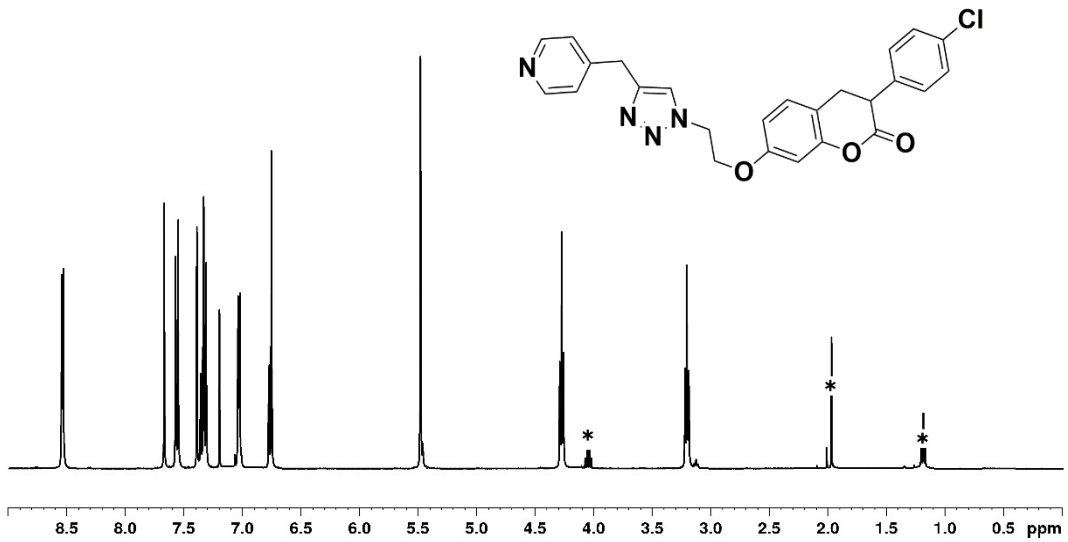

Figure S10. 400 MHz ^{1}H-NMR of **L$_{10}$** (in $CDCL_3$, ✱ = solvent residual peak).

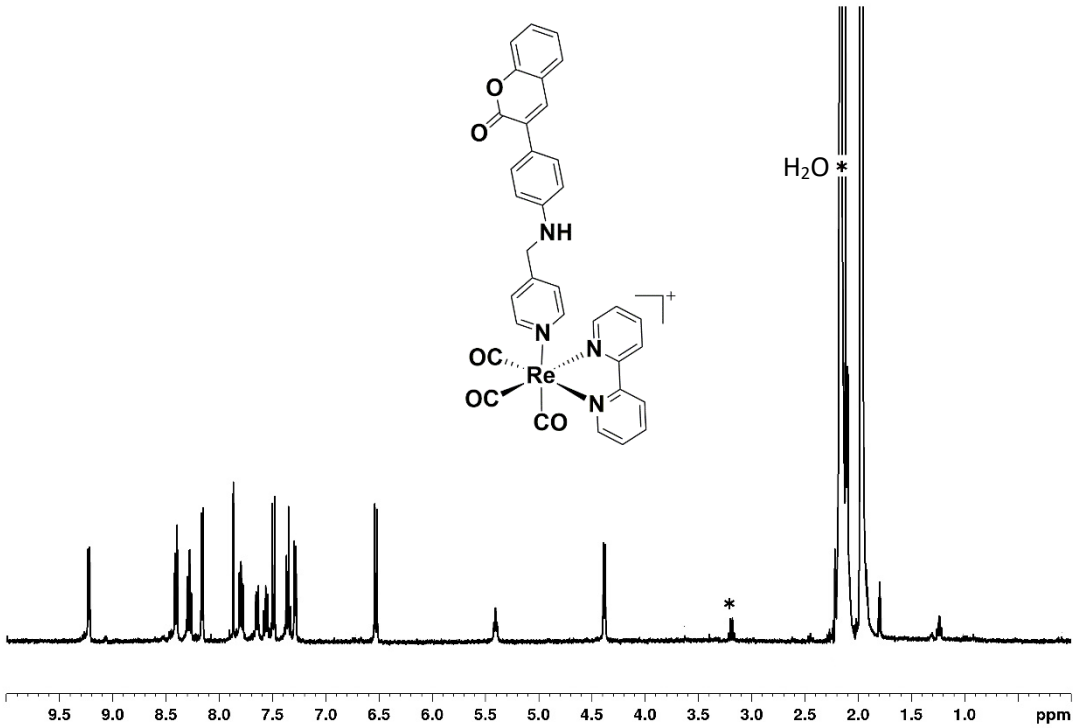

Figure S11. 400 MHz ^{1}H-NMR of **ReL$_1$** (in CD_3CN, ✱ = solvent residual peak)

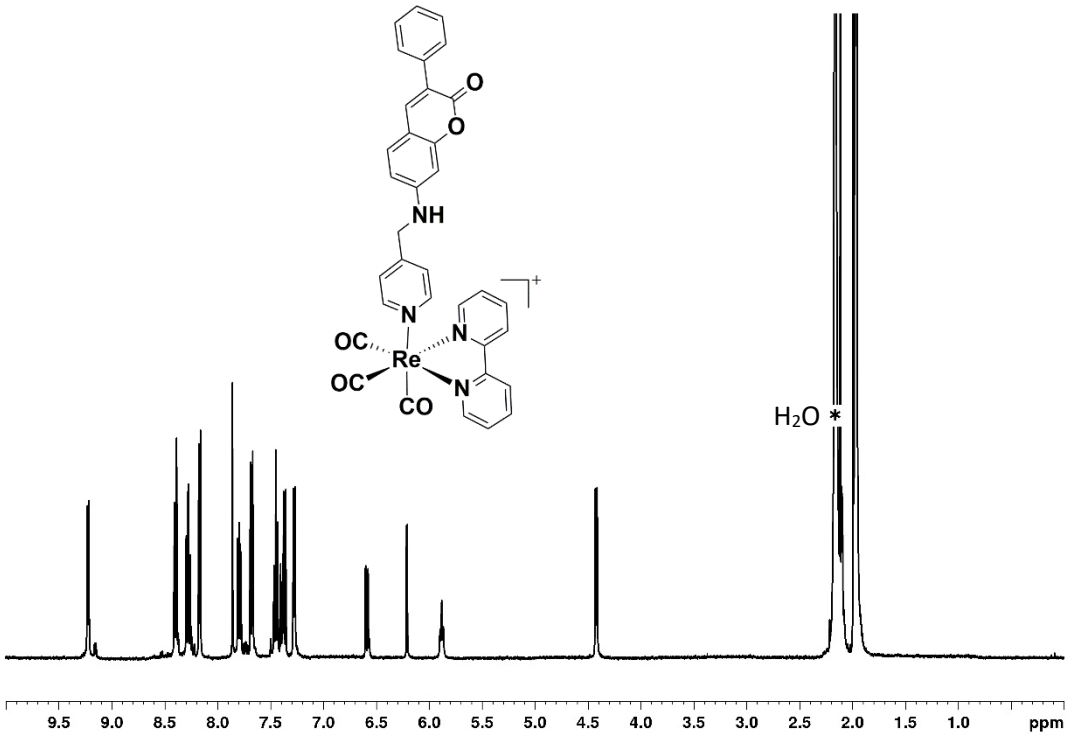

Figure S12. 400 MHz ^{1}H-NMR of **ReL$_2$** (in CD_3CN, ✱ = solvent residual peak)

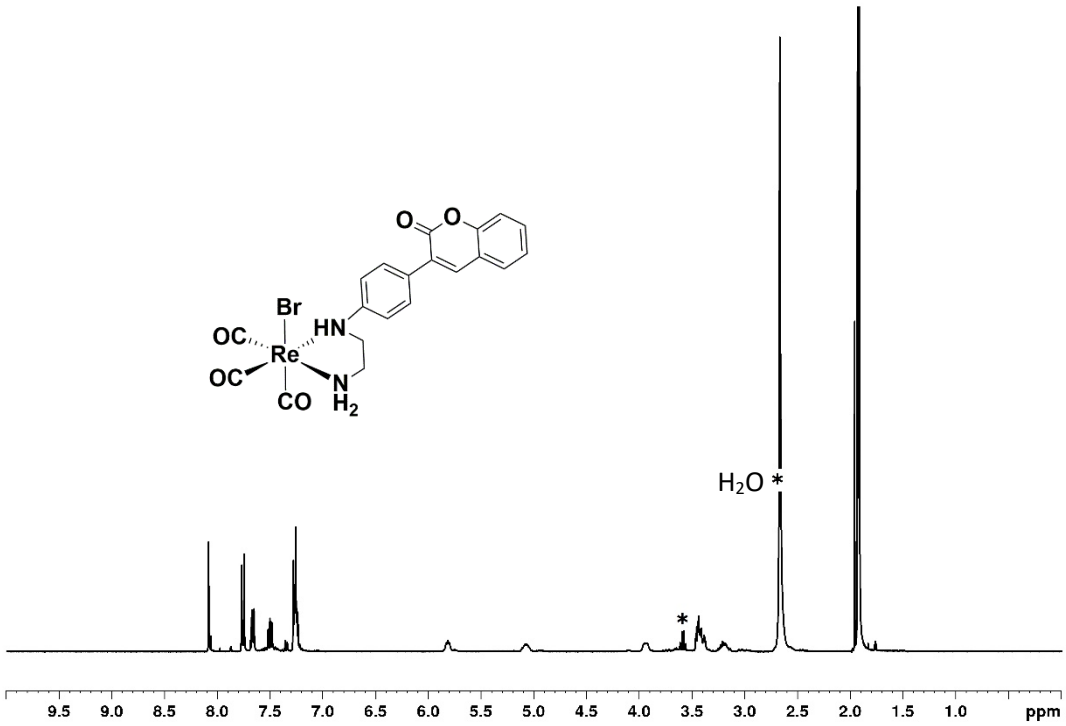

Figure S13. 400 MHz ^{1}H-NMR of **ReL$_3$** (in $(CD_3)_2CO$, ✱ = solvent residual peak)

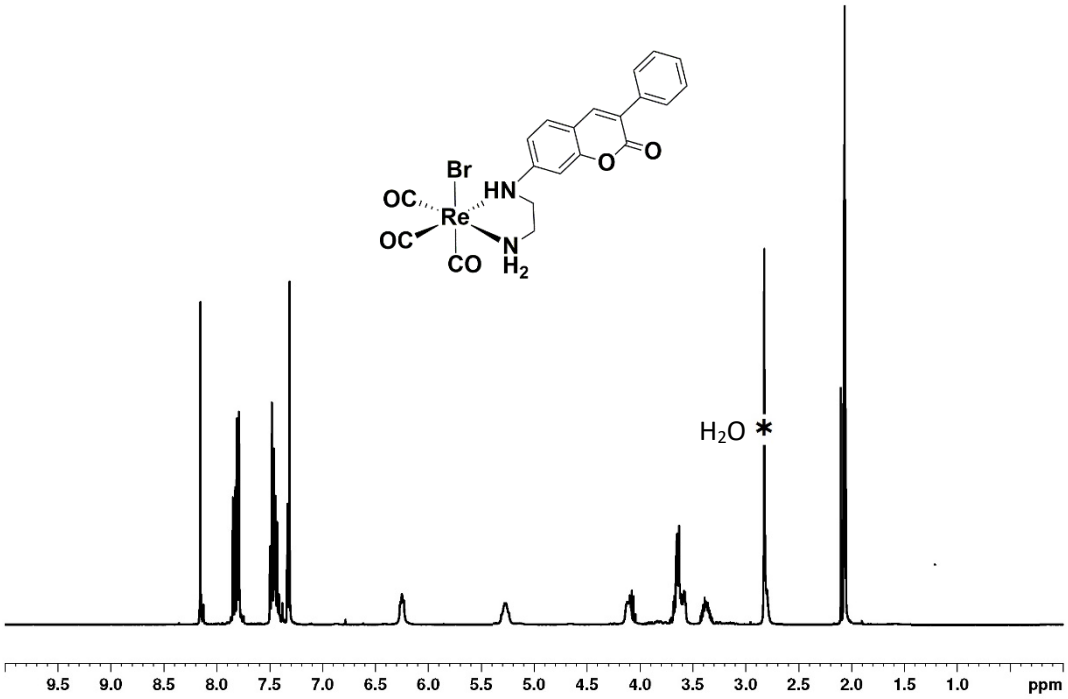

Figure S14. 400 MHz ^{1}H-NMR of **ReL$_4$** (in $(CD_3)_2CO$, ✱ = solvent residual peak)

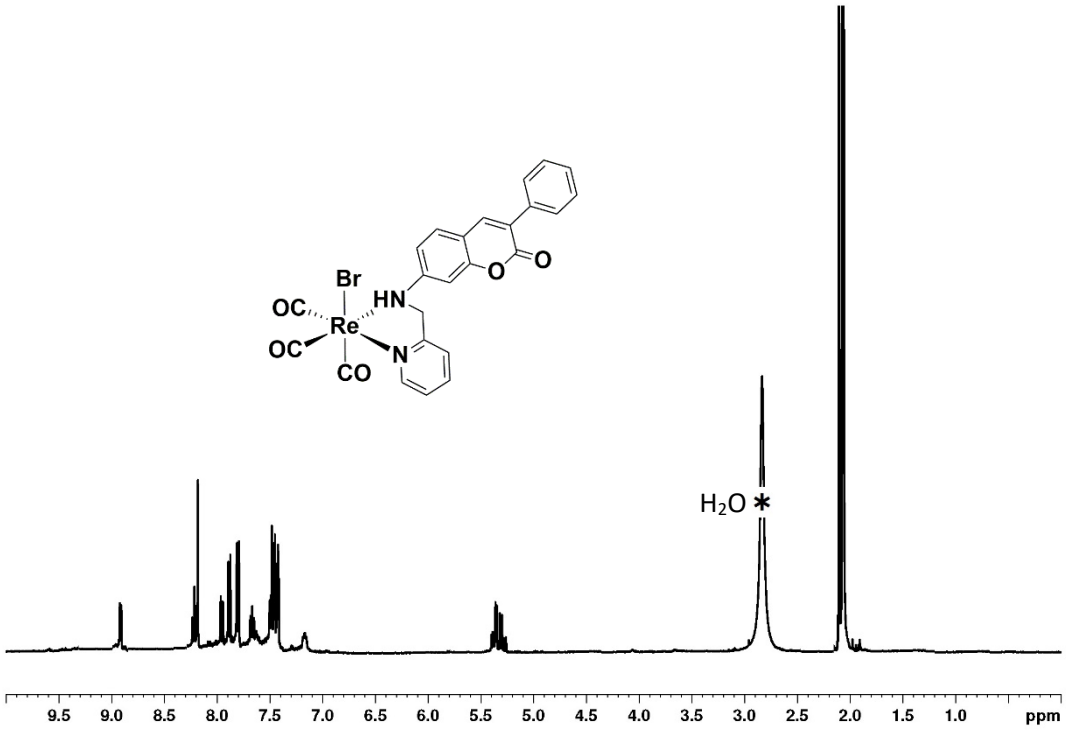

Figure S15. 400 MHz ^{1}H-NMR of **ReL$_5$** (in $(CD_3)_2CO$, ✱ = solvent residual peak)

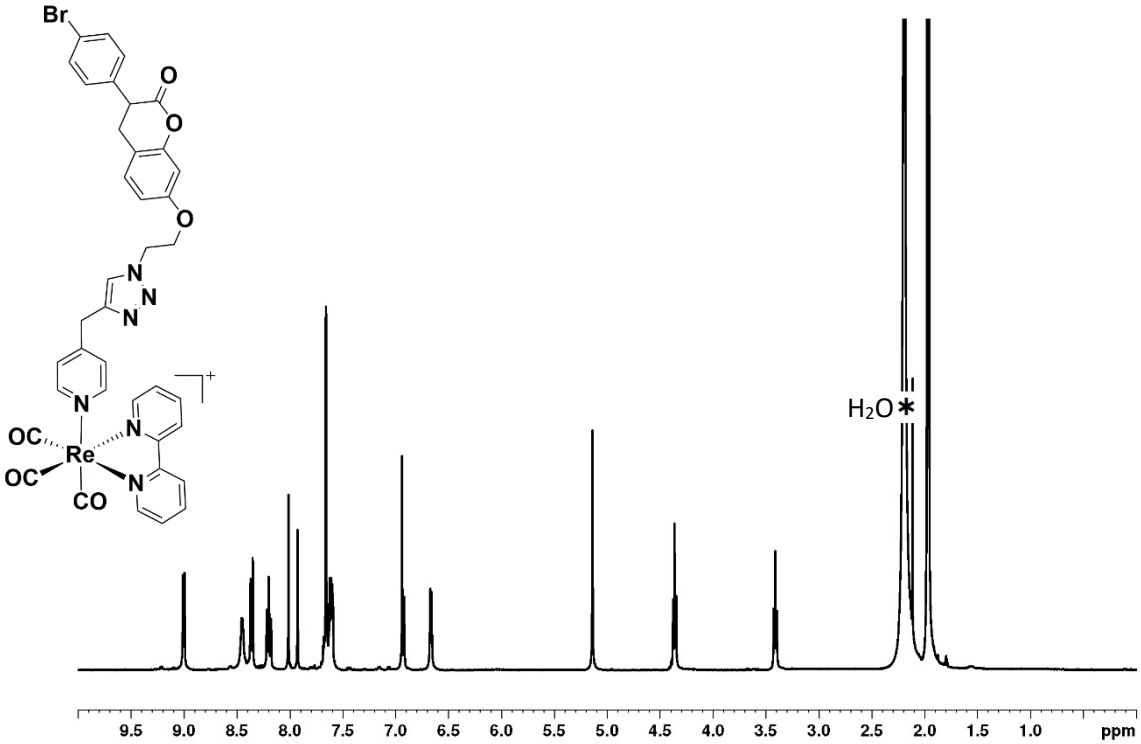

Figure S16. 400 MHz ^{1}H-NMR of **ReL$_6$** (in CD_3CN, ✱ = solvent residual peak)

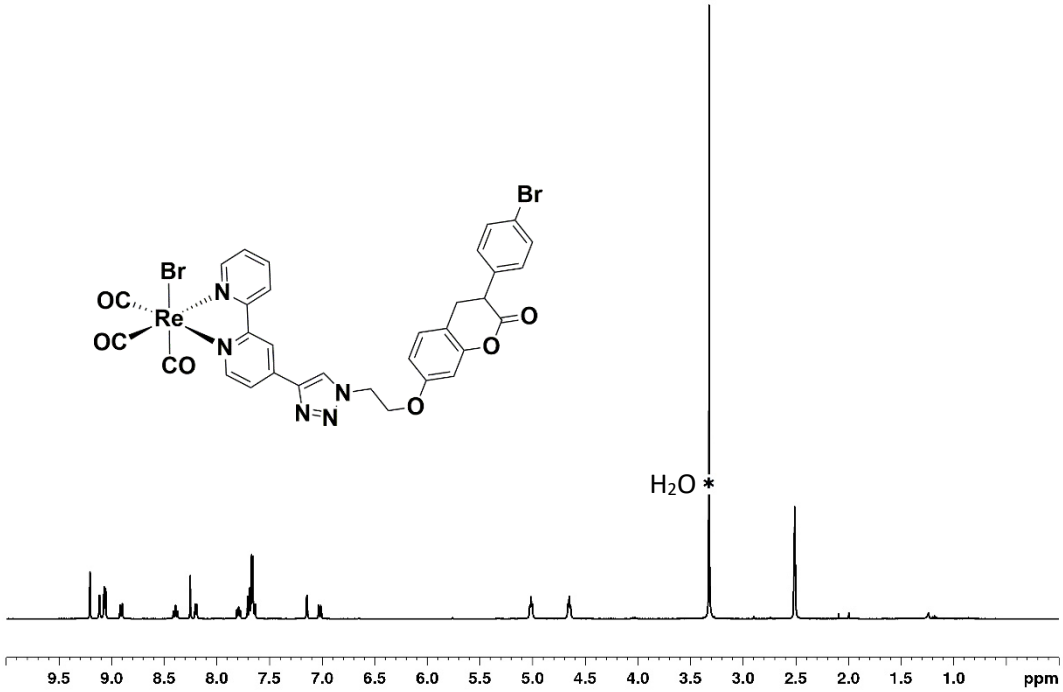

Figure S17. 400 MHz ^{1}H-NMR of **ReL$_7$** (in $(CD_3)_2SO$, ✱ = solvent residual peak)

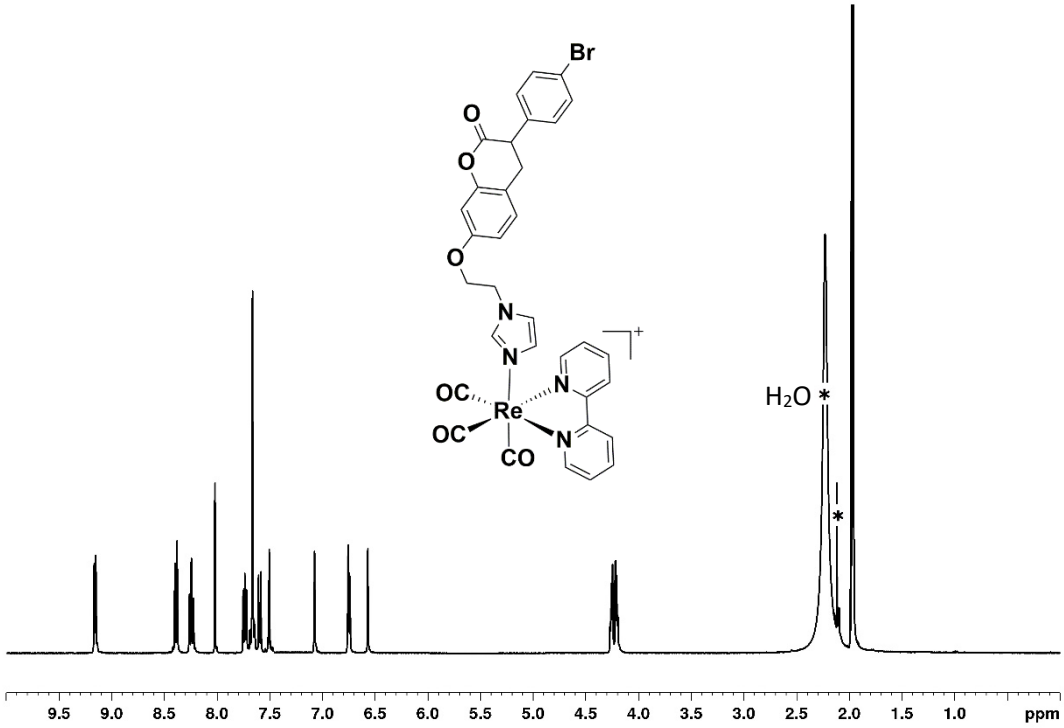

igure S18. 400 MHz ^{1}H-NMR of **ReL$_8$** (in CD_3CN, ✱ = solvent residual peak)

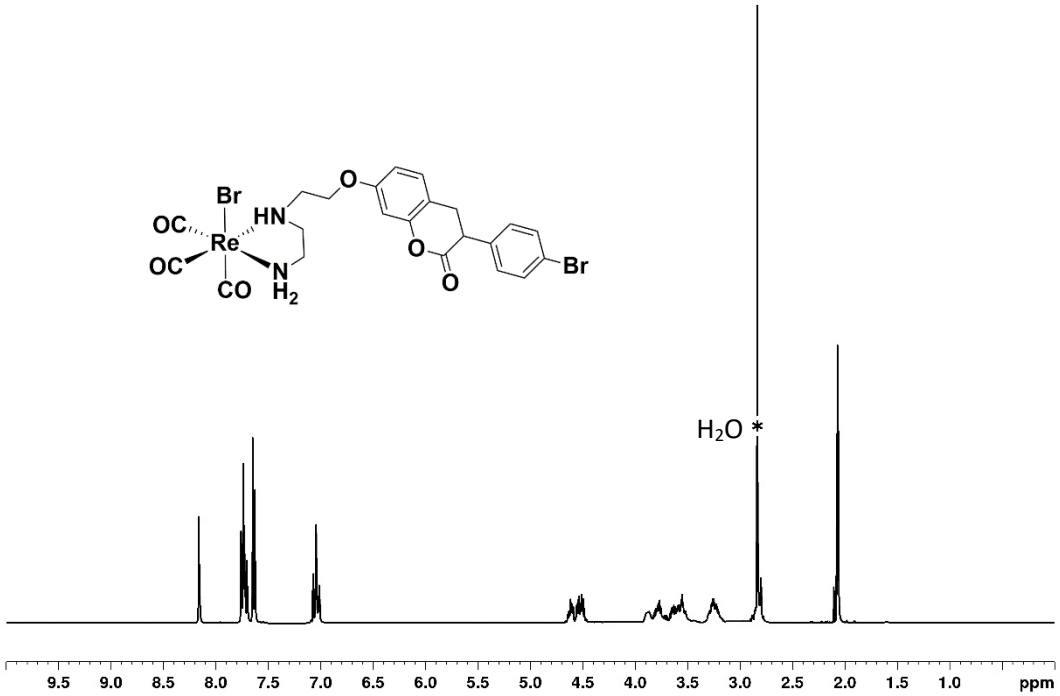

Figure S19. 400 MHz ^{1}H-NMR of **ReL$_9$** (in $(CD_3)_2CO$, ✱ = solvent residual peak)

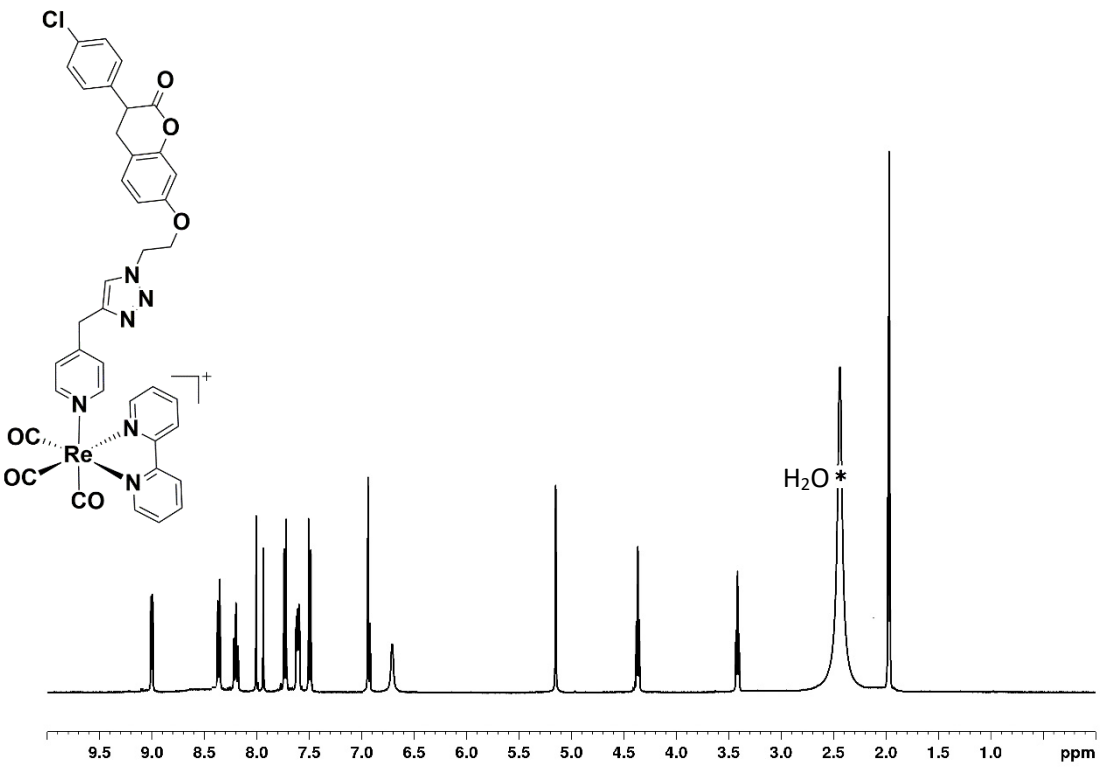

Figure S20. 400 MHz ^{1}H-NMR of **ReL$_{10}$** (in CD_3CN, ✱ = solvent residual peak)

Table S1. Antimicrobial activity of 3-arylcoumarin ligands (μM) against Gram-positive and Gram negative bacterial and fungal strains.

Ligands	***S. aureus* A TCC 25923**	***P. aeruginosa* NCTC 10332**	***C. albicans* ATCC 10231**	***C. parapsilosis* ATCC 22019**	***C. glabrata* ATCC 2001**	***C. krusei* ATCC 6258**	***MRC-5 cells***
L1	>609	>609	>609	>609	>609	>609	672
L2	>609	>609	>609	>609	>609	>609	76
L3	>713	>713	>713	>713	>713	356	53
L4	713	>713	713	713	100	178	35
L5	>609	>609	>609	>609	>609	>609	152.2
L6	>397	>397	200	25	50	200	496
L7	>800	>800	>800	>800	>800	>800	8
L8	>800	>800	>800	>800	>800	>800	145
L9	50	400	25	25	25	25	35
L10	>800	>800	>800	800	800	800	225

Table S2. IC50 values of ReL# complexes on MRC-5 cells.

Complexes	**MRC-5 (μM)**
ReL_1	14.0 ± 0.4
ReL_2	3.5 ± 0.1
ReL_3	13.5 ± 0.4
ReL_4	7.5 ± 0.1
ReL_5	4.5 ± 0.1
ReL_6	21 ± 1
ReL_7	30 ± 1
ReL_8	4.5 ± 0.2
ReL_9	17.5 ± 0.5
ReL_{10}	17.5 ± 0.2
Linezolid	nd
Vancomycin	nd

Table S3. Crystallographic details

	L_1	**L_2**	**L_5**	**L_6**	**L_8**	**ReL_2**	**ReL_5**	**ReL_7**
Formula	$C_{21}H_{16}N_2O_2$	$C_{22}H_{17}Cl_3N_2O_2$	$C_{42}H_{32}N_4O_4$	$C_{25}H_{19}BrN_4O_3$	$C_{20}H_{15}BrN_2O_3$	$C_{35}H_{25.5}F_6N_{4.5}O_5PRe$	$C_{24}H_{14}BrN_2O_5Re$	$C_{32}H_{20}Br_2N_5O_6Re$
M_W	328.36	447.72	656.71	503.35	411.25	920.27	676.48	916.55
T [K]	250(2)	200(2)	250(2)	250(2)	200(2)	200(2)	250(2)	200(2)
Lattice	monoclinic	triclinic	monoclinic	triclinic	triclinic	monoclinic	triclinic	monoclinic
Space group	$P2_1/c$	P-1	$P2_1/c$	P-1	P-1	$P2_1/c$	P-1	$P2_1/c$
Z	4	2	4	2	2	4	2	4
a [Å]	11.9096(14)	5.7830(3)	26.693(4)	6.1355(9)	7.2714(11)	10.7780(2)	6.8256(3)	31.5785(3)
b [Å]	12.0649(11)	10.4682(7)	6.2512(6)	11.1737(13)	8.4220(13)	17.1490(4)	10.2784(5)	12.9371(4)
c [Å]	11.4744(15)	17.6816(11)	20.184(3)	16.765(2)	14.512(2)	18.6102(4)	16.4526(7)	8.2504(13)
α [°]	90	92.833(5)	90	80.570(9)	86.872(12)	90	103.417(4)	90
β [°]	99.950(10)	98.656(5)	105.956(12)	82.188(11)	82.538(11)	94.801(2)	92.130(4)	91.534(3)
γ [°]	90	99.429(5)	90	75.013(10)	71.409(11)	90	103.568(4)	90
V [Å^3]	1623.9(3)	960.875	3238.3(8)	1090.0(3)	835.1(2)	3427.69(13)	1086.28(9)	3369.4(5)
d_{calcd} [g/cm^3]	1.343	1.429	1.347	1.534	1.635	1.783	2.068	1.807
R_1, wR_2	0.0525, 0.1325	0.0393, 0.1037	0.1072, 0.2401	0.0662, 0.1084	0.0691, 0.1734	0.0616, 0.1583	0.0258, 0.0546	0.0813, 0.2181

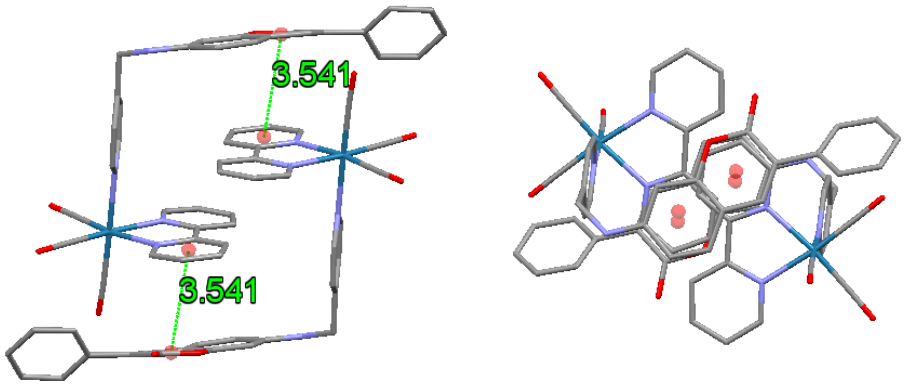

ReL_2

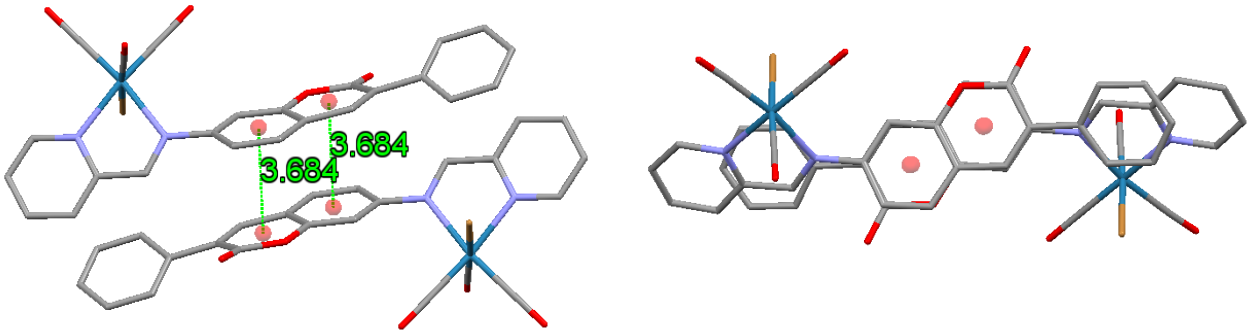

ReL_5

Figure S21. π-stacking interactions observed in solid state structure of ReL_2 (top) and ReL_5.

In order to assign these transitions we performed DFT calculations. Geometry optimization of the complexes was performed in the gas phase while TDDFT calculations were all performed in acetonitrile using the polarizable continuum model. Given the work of Minenkov [68], we decided to use the standard density functional wB97XD, accounting for dispersion, in combination with the SDD basis set. The results of this analysis reveal that the 330 nm transition can be attributed to an intense intraligand transition of the 3-arylcoumarin (3-AC) ligands (LC, π–π*, Figure 2). The shoulder at 310 nm relates to a HOMO-3 to -9 → LUMO/+1 theoretical transition involving orbitals of mixed p(O), of CO ligands, -π(ReCO)-π(3-AC) → π*(3-AC) for *fac*-[Re(CO)$_3$(L⌒L)Br] complexes and predominantly π(bpy)-π(3-AC) → π*(bpy) for *fac*-[Re(CO)$_3$(bpy)L]$^+$ species.

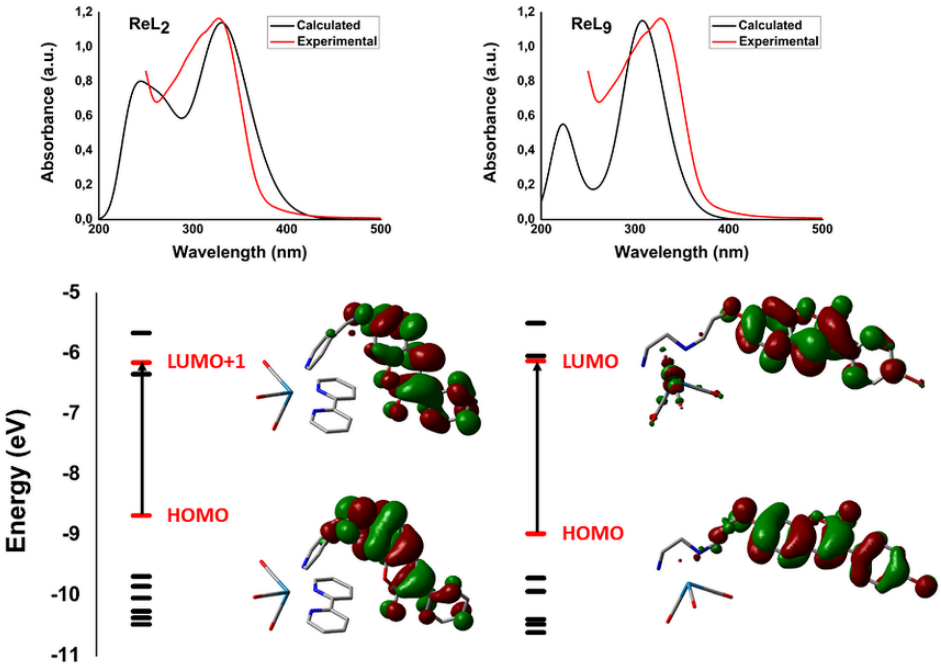

Figure 22a. Calculated HOMO/LUMO energy diagram of complexes ReL$_2$ (left) and ReL$_9$. The most prominent MOs involved in transition under the visible energy band at 330 nm and their diagrams are shown.

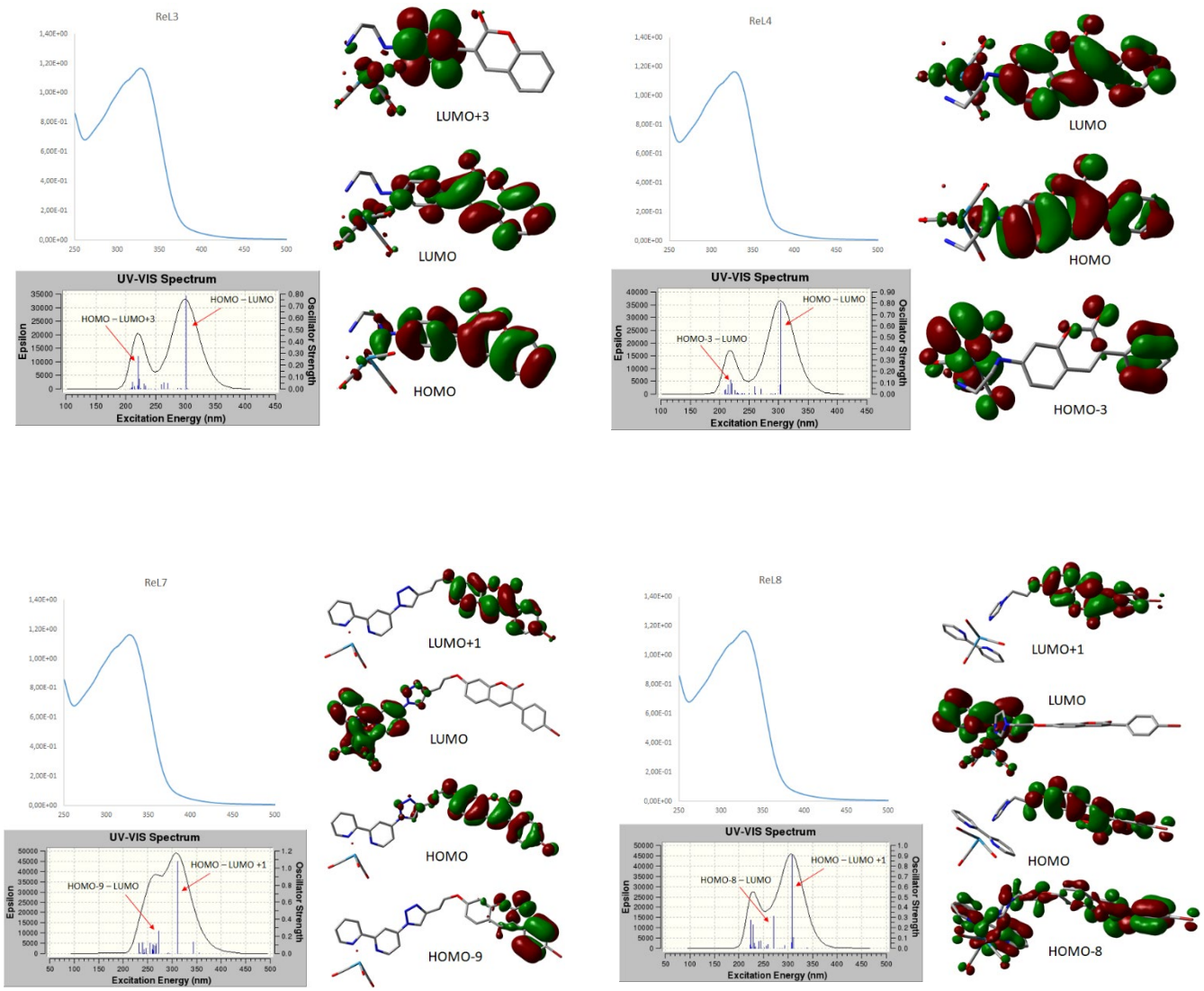

Figure S22b. Selected examples of calculated electronic spectra of $ReL_{\#}$ complexes. The most prominent MOs (i.e. highest oscillator strength/value) involved in the indicated transition are shown.

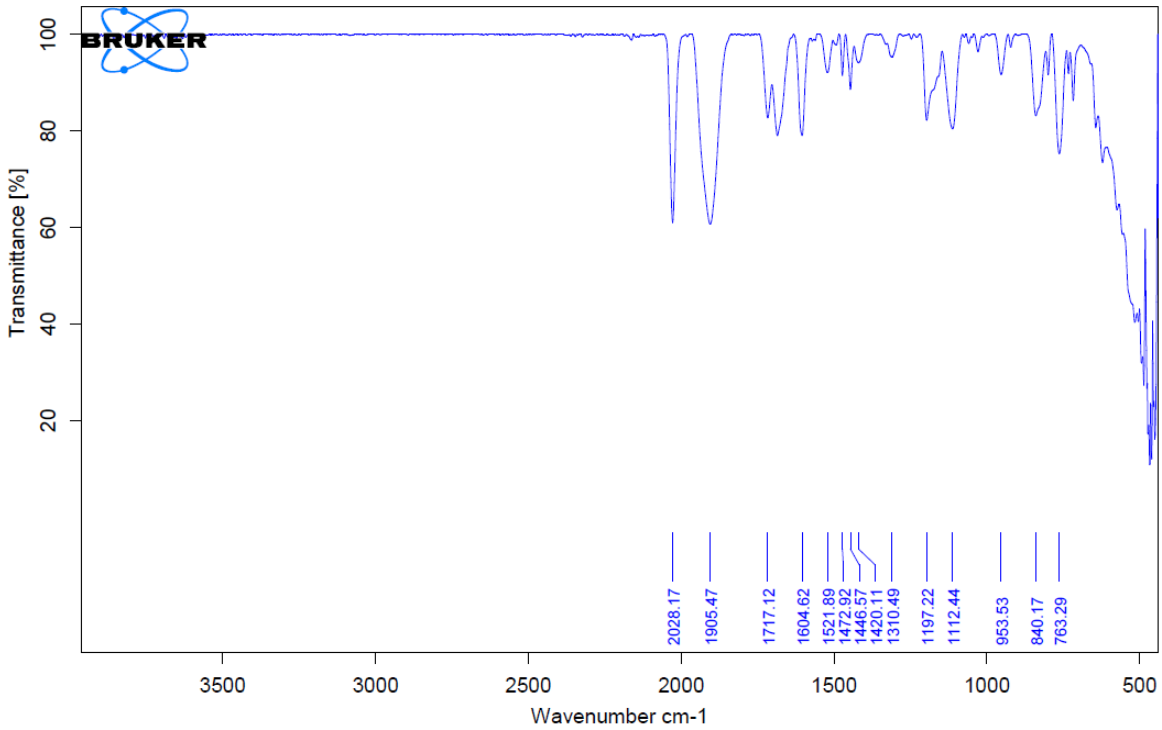

Figure S23. IR spectrum (solid state) of ReL1

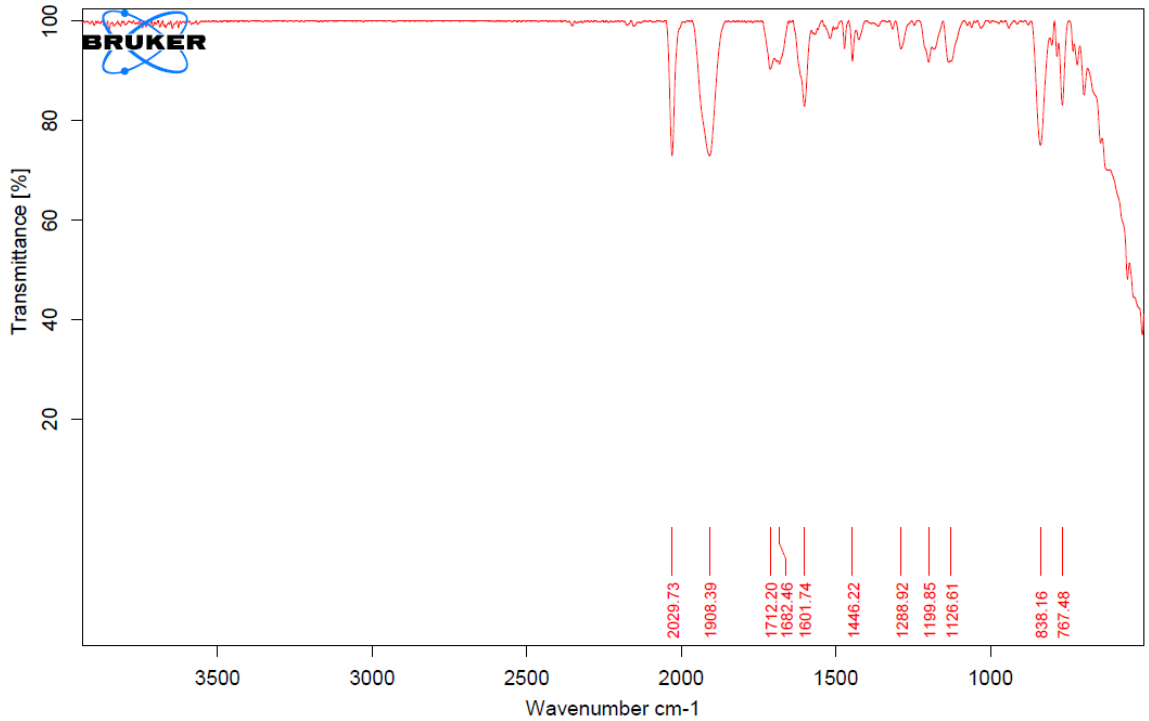

Figure S24. IR spectrum (solid state) of ReL2

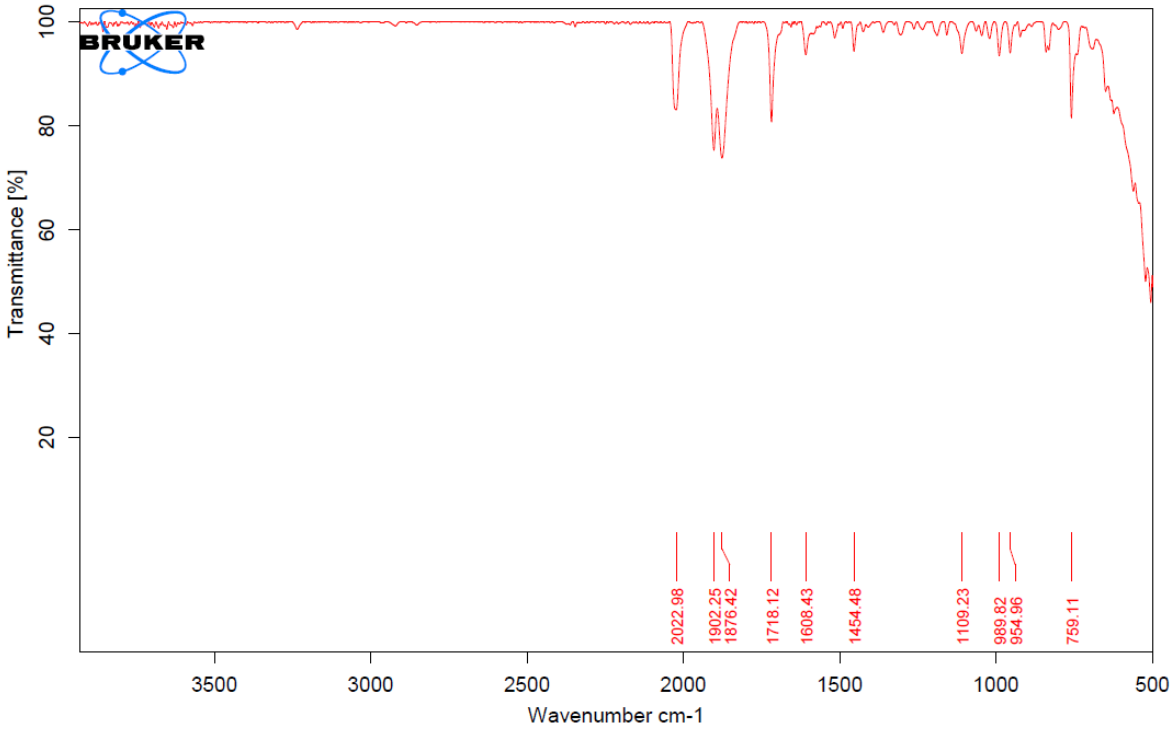

Figure S24. IR spectrum (solid state) of ReL3

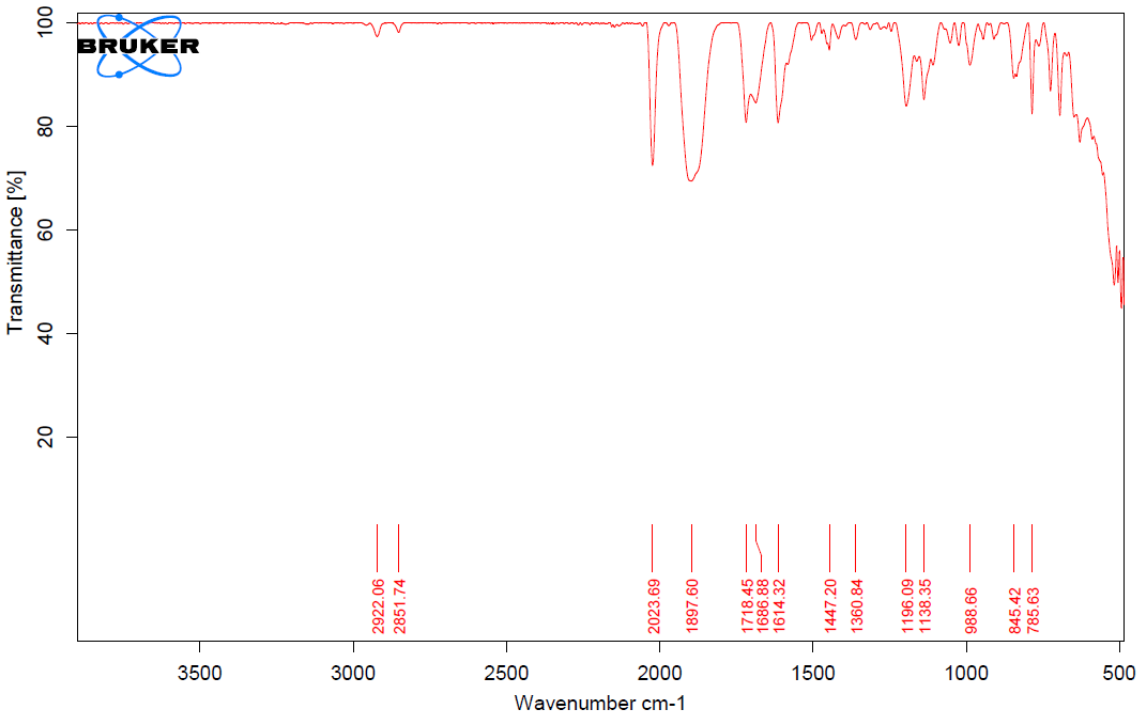

Figure S25. IR spectrum (solid state) of ReL4

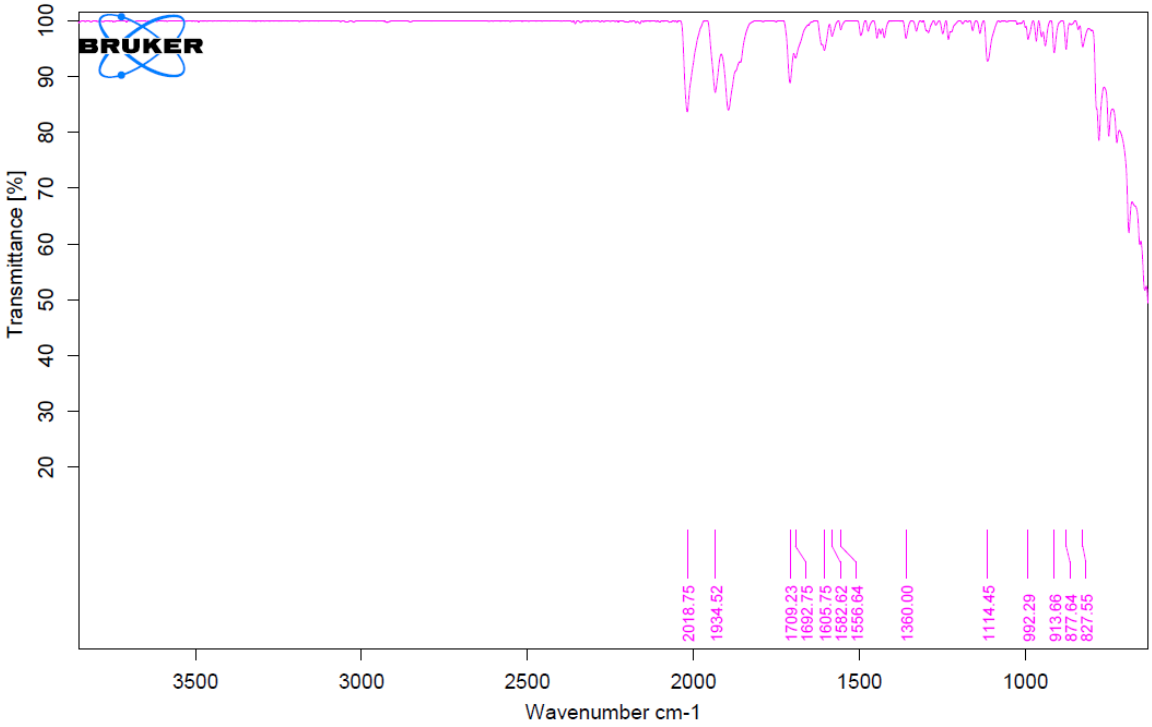

Figure S26. IR spectrum (solid state) of ReL5

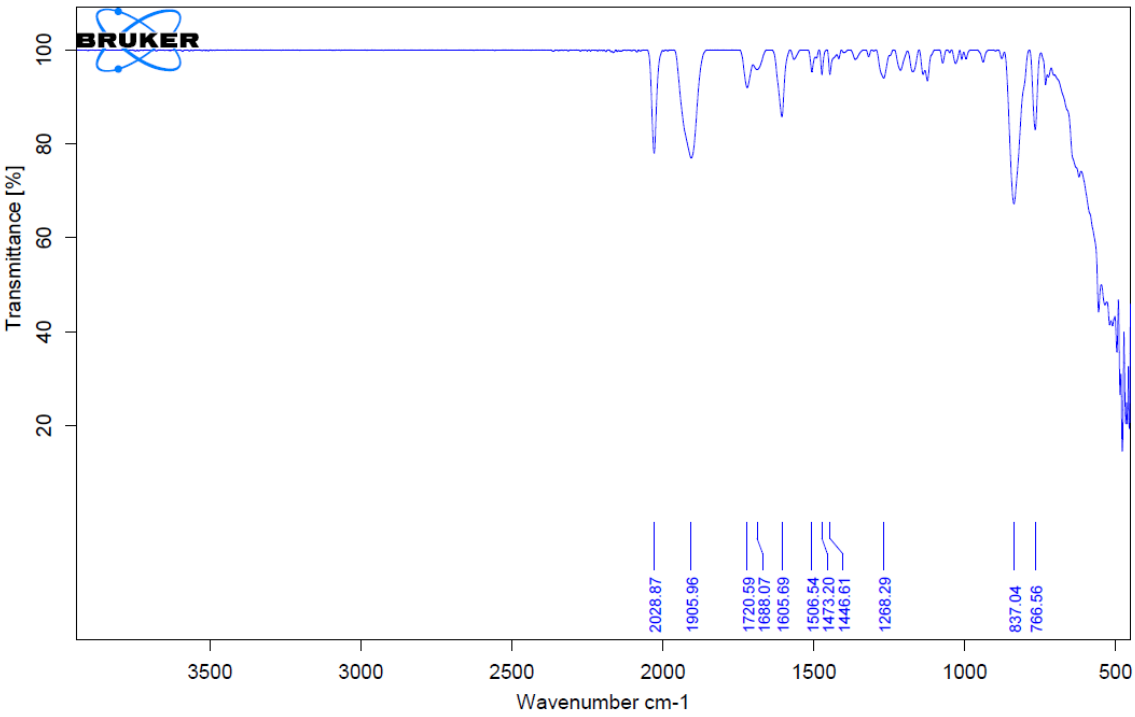

Figure S27. IR spectrum (solid state) of ReL6

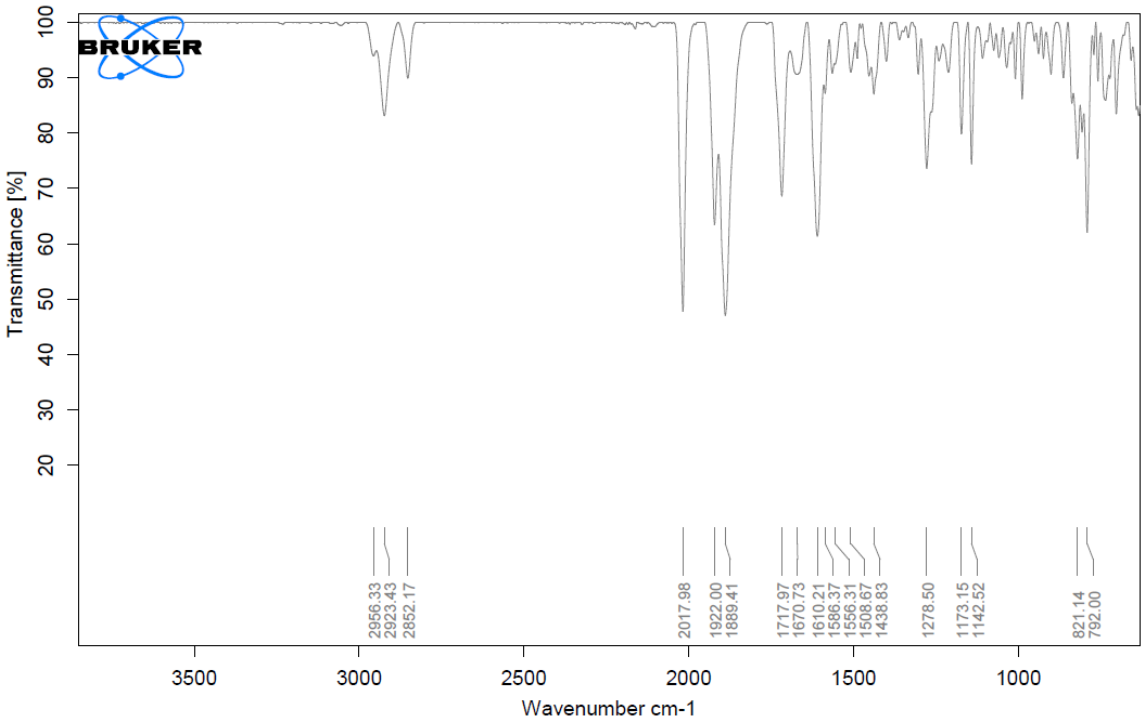

Figure S28. IR spectrum (solid state) of ReL7

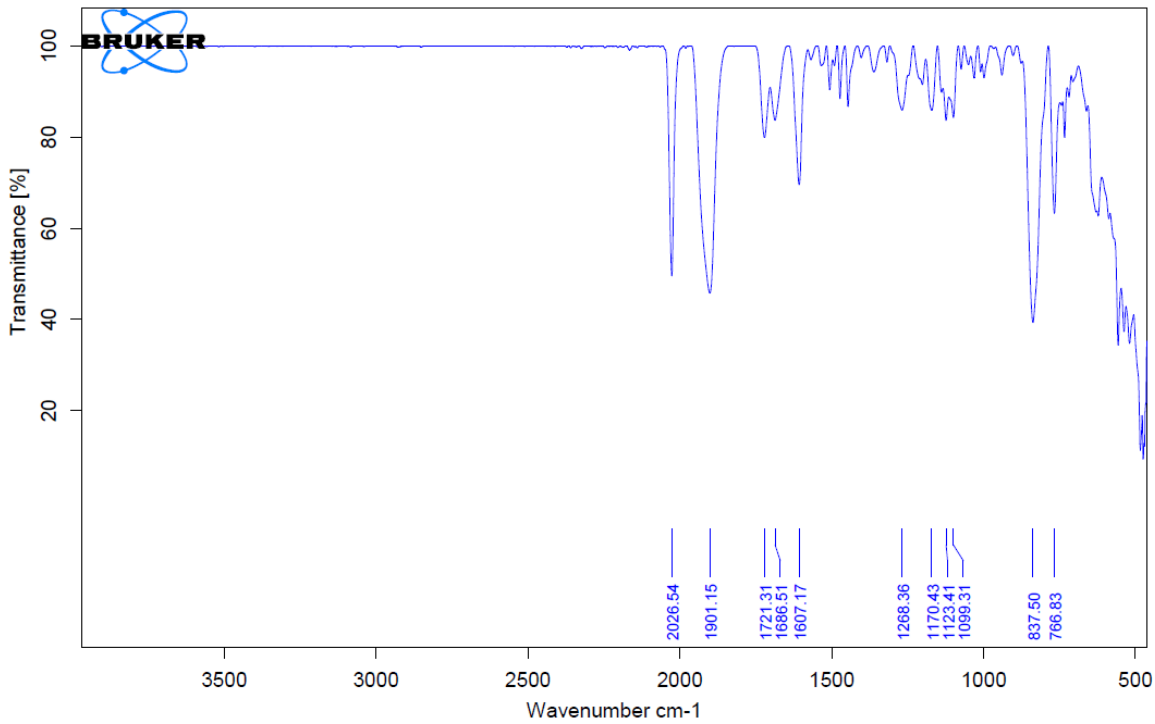

Figure S29. IR spectrum (solid state) of ReL8

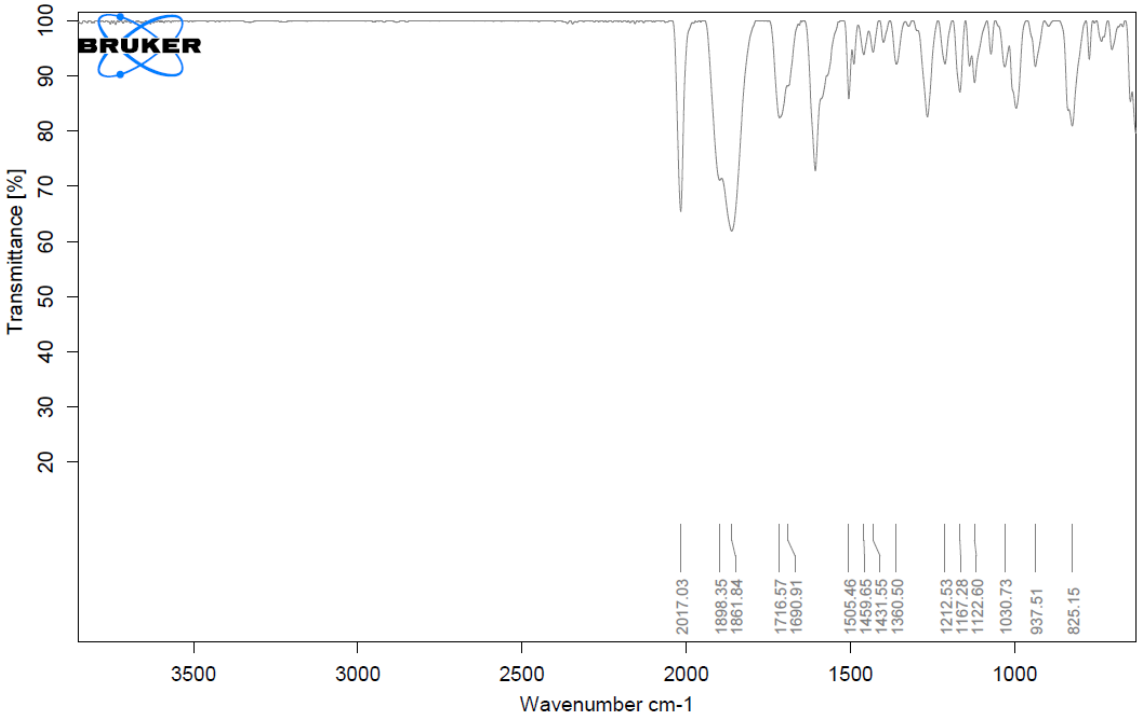

Figure S30. IR spectrum (solid state) of ReL9

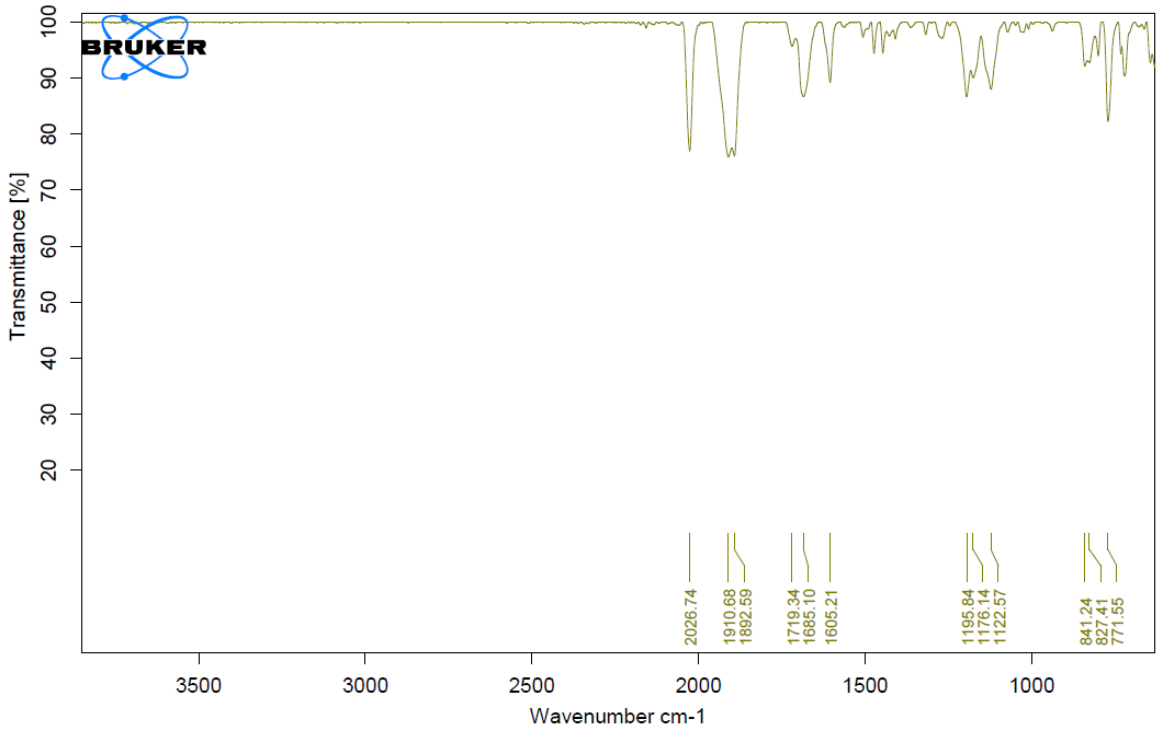

Figure S31. IR spectrum (solid state) of ReL10

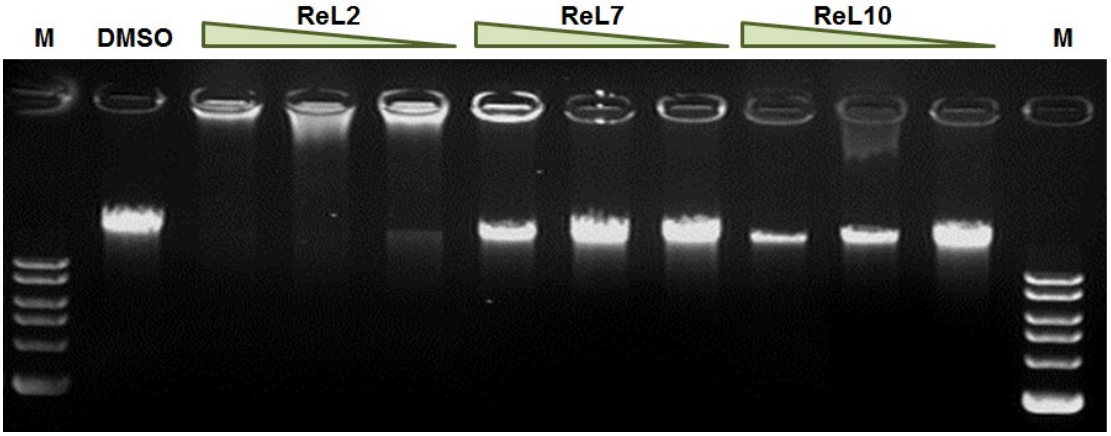

Figure S32. *In vitro* interaction of selected $ReL_{\#}$ complexes with lambda bacteriophage DNA (20 ng/µL, 37 °C, 2 h in 10 mM Tris-Cl, pH 8.5). Concentrations of complex ReL_1 are 400, 200 and 100 µM.